Technical Report

Muographic Study of the Palazzone Necropolis (Perugia-Italy)

D. Borselli,[1,2] T. Beni,[2,3] L. Bonechi,[2] M. Bongi,[2,4] R. Ciaranfi,[2] V. Ciulli,[2,4] R. D'Alessandro,[2,4] L. Fanò,[1,5] C. Frosin,[2,4] S. Gonzi,[2,4] L. Lombardi,[3] L. Melelli,[1] A. Paccagnella,[2,4] and M. A. Turchetti[6]

[1]*University of Perugia, Department of Physics and Geology, Perugia, Italy*

[2]*INFN, Florence Division, Florence, Italy*

[3]*University of Florence, Department of Earth Sciences, Florence, Italy*

[4]*University of Florence, Department of Physics and Astronomy, Florence, Italy*

[5]*INFN, Perugia Division, Perugia, Italy*

[6]*Ministry of Culture Regional Directorate of Museums Umbria, Necropolis of Palazzone, Perugia, Italy*

Corresponding author: D. Borselli
Email address: borsellid@fi.infn.it

Abstract

The Palazzone Necropolis, located southeast of the hill of Perugia (Italy), is an Etruscan archaeological site open to the public, and well-known thanks to the numerous finds and its (∼)200 tombs from the Hellenistic age and 5 from the Archaic period. The most important tomb is represented by the Volumni Hypogeum. The Palazzone Necropolis is also defined as an archaeogeosite as it has been the subject of geological studies which, through the observation of the walls of the tombs, has made it possible to expand the geological framework for the interpretation of the formation of the Perugia hill. However, in the Palazzone Necropolis, the presence of other tombs is not excluded, especially in the eastern area of the archaeological site which is currently not open to visitors. The muography technique, thanks to the great penetrating power of atmospheric muons, fits into this context for the noninvasive identification of undiscovered cavities. This contribution will present the preliminary results of the muographic campaign carried out at the Palazzone Necropolis in which the observation of an entire hill was carried out. The results are also inserted in a geological context for the verification of the densities of the sediments that are present in this territory.

Keywords: muon radiography, archaeology, cosmic rays
DOI: 10.31526/JAIS.2024.467

1. INTRODUCTION: MUON RADIOGRAPHY TECHNIQUE AND IMAGING METHODOLOGY

The transmission muography technique allows, through the penetrating power of atmospheric muons, obtaining a noninvasive transmission image of the target in a similar way to X-ray radiography. With this technique, it is possible to monitor the inside of large structures such as mountains, pyramids [1], or volcanoes [2, 3, 4, 5]. The detectors used for these measurements are trackers, i.e., detectors developed in the field of high energy physics that allow us to reconstruct and count the number $N_\mu(\theta, \varphi)$ of tracks associated with muons coming from a certain direction of observation identified by the zenith angle θ and the azimuth angle φ. This quantity depends on the flux $\Phi(\theta, \varphi)$ of atmospheric muons coming from the direction identified by the solid angle $\Delta\Omega$, on the acquisition time Δt, and on the characteristics of the detector (efficiency ϵ and sensitive surface of the detector A_{eff} perpendicular to the direction of view) following the following relationship: $N_\mu(\theta, \varphi) = \Phi(\theta, \varphi) \cdot \Delta t \cdot \epsilon(\theta, \varphi, t) \cdot A_{\text{eff}}(\theta, \varphi) \cdot \Delta\Omega$.

Atmospheric muons [6] ($m_\mu \sim 105.6\,\text{MeV/c}^2 \simeq 200\,m_e$, where m_μ and m_e are, respectively, the mass of muon and electron) are the most penetrating charged particles generated by the interaction of primary cosmic rays with our atmosphere and one of the few charged particle types that reach the Earth's surface. The energy spectrum of atmospheric muons is peaked at about ∼3 GeV reaching values of the order of TeV and shifts toward higher energy values the more the observation direction is inclined with respect to the vertical direction [6, 7]. Furthermore, the muon flux varies with the zenith angle as $\propto \cos^n(\theta)$ where $n = 2$ for $E_\mu \sim 3\,\text{GeV}$. The average integrated rate over the whole solid angle at sea level is about $100\,\text{Hz/m}^2$ [6]. The rate depends on the altitude, the latitude, the longitude, and the atmospheric conditions of temperature and pressure [7]. The muon is a charged particle with a high penetrating power in matter, being the radiative losses of *bremsstrahlung* and of pair production ($e^- e^+$) reduced for particles with large masses.

The imaging methodology is implemented following three phases:

(i) *target measurement*: performed at the site of interest by pointing the detector toward the observation structure (target) at the angles $(\overline{\theta}, \overline{\varphi})$;

(ii) *free-sky measurement*: performed without objects between the detector and the sky, pointing the detector at the same angles as the target measurement $(\overline{\theta}, \overline{\varphi})$;

(iii) *simulations*: they must describe a realistic model of cosmic ray flux on the ground, a geometric model of the target structure, the position of the detector (the same as the target measurement), and the pointing direction $(\overline{\theta}, \overline{\varphi})$.

It can be understood how important it is to estimate with good precision the position of the detector in the measurement site and its pointing direction, so as to be able to reproduce it in the free-sky measurement (pointing direction) and in the simulations (position and pointing direction) and avoid shifts between measurements and simulations.

By comparing the results of the first two points, we obtain the measured transmission of muons:

$$t_{\text{meas}}(\theta, \varphi) = \frac{\Phi_{\text{target}}(\theta, \varphi)}{\Phi_{\text{free-sky}}(\theta, \varphi)} = \frac{N_{\mu_{\text{target}}}(\theta, \varphi)}{N_{\mu_{\text{free-sky}}}(\theta, \varphi)} \cdot \frac{\Delta t_{\text{free-sky}}}{\Delta t_{\text{target}}}, \tag{1}$$

where it was assumed, in the second equality, that the efficiency of the detector and its geometrical conditions remained the same in the two measurements. The transmission value (dimensionless and less than unity) depends not only on the materials that make up the target but also on the geometry of the structure of interest; in particular, it depends on the opacity $X(\theta, \varphi) = \overline{\rho}(\theta, \varphi) \cdot l(\theta, \varphi)$, where $\overline{\rho}$ is the average density and l the material depth encountered in the (θ, φ) direction. Therefore, in order to take into account the known details of the target and to be able to convert the measured muon transmission distributions into average density distributions, a comparison with detailed simulations that consider the known geometry of the target is carried out. From the simulations, we obtain the expected muon transmission $t_{\text{simu}}(\theta, \varphi)$.

By comparing the measurements with the simulations, it is possible to identify any anomalies with respect to the known geometry of the target. Furthermore, by varying the density of the simulation, it is possible to estimate the average density value of the materials encountered. A two-dimensional map of average density is generated. In the particular case of the search for cavities in an archaeological site, areas will be sought in which the density is significantly lower than the density of the surrounding materials, since the average density defect due to the presence of cavities affects the opacity by lowering it proportionally to the average density itself.

To obtain three-dimensional information and therefore find the distance between the detector and the detected anomaly, inversion and triangulation algorithms [8, 9, 10, 11] are used, which implies being able to carry out more than a single measurement, or exploiting a single measurement using focusing algorithms [12, 13, 14].

2. EXPERIMENTAL APPARATUS: THE MIMA MUON TRACKER

The MIMA (Muon Imaging for Mining and Archaeology) tracker [15, 16] was assembled between 2016 and 2017 by the muography group of the INFN of Florence division and the Department of Physics and Astronomy of the University of Florence and until now has acquired data in geological [17], archaeological [18], and civil security [19] applications. MIMA consists of 3 tracker modules X-Y made of scintillator bars with triangular sections arranged to form a sensitive plane of dimensions $(40 \times 40)\,\text{cm}^2$. The bars X are orthogonal to bars Y. Each triangular face of a bar is coupled with a SiPM (*Silicon PhotoMultiplier*) which collects the weak light signals developing inside the bar and carries them to an electronic board. The modules are enclosed in an aluminum mechanics on which the electronic boards are housed. The details of the electronics and trigger logic are described in some previous works [15, 16]. Given the triangular shape of the bars, it is possible to reconstruct the impact point of the particle in the scintillator plane through a center of gravity algorithm. The spatial resolution of the single plane is about 1.6 mm, and the angular resolution is about 6 mrad. The modules are housed in an aluminum cube of approximate dimensions $(50 \times 50 \times 50)\,\text{cm}^3$ with a weight of about 80 kg and mechanics that allow the altazimuth orientation. These characteristics make MIMA a detector particularly suitable for installation in difficult-to-access places such as shafts or tunnels. Figure 1 shows MIMA measuring at the Palazzone Necropolis.

3. THE PALAZZONE NECROPOLIS

The Palazzone Necropolis [20] is located near the Perugia hill southeast of the city and is currently open to visitors. The necropolis contains about 200 Etruscan tombs (Figure 2(a)) from the Hellenistic period (3rd and 1st century BC) and 5 from the Archaic period (second half of the 6th–early 5th century BC). The most significant tomb is the Volumni Hypogeum belonging to the Velimna family which has a structure similar to that of a Roman house: a main room from which other secondary rooms branch off. The necropolis tombs are found at an average depth of a few meters after a corridor that starts from the surface, and in some cases, as happens for the Volumni Hypogeum, it is possible to reach depths of around 10 m. The tourist route is articulated both outside, where it is possible to visit and enter some tombs directly from the surface, and inside where the Antiquarium and warehouse rooms house many archaeological finds and laboratories.

The necropolis represents an archaeogeological site [21]: in fact, the walls of the tombs are a three-dimensional environment within which it is possible to study the area and give a geological interpretation of the territory. These geological studies highlight the presence of two main units [21, 22]: the Volumni unit and the Palazzone unit (Figure 2(b)). The two units are made up of sands and conglomerates, but while in the Volumni unit the conglomerates prevail over the sands, in the Palazzone unit the sands prevail over the conglomerates. The typical densities of the materials that make up the area are in the range of 1.8–2.3 g/cm^3 with slightly higher values for the Volumni unit.

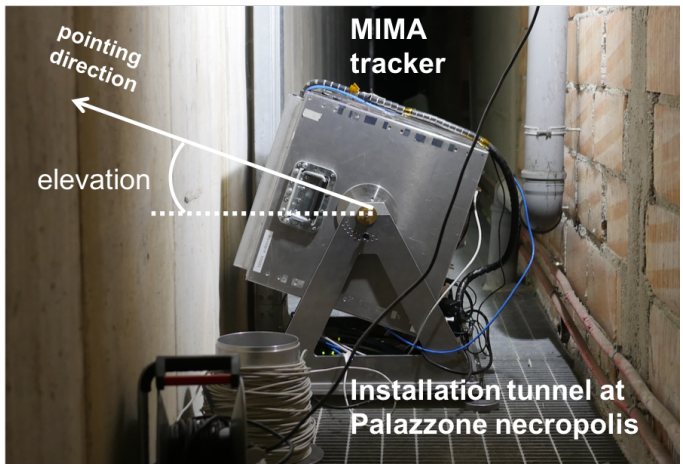

FIGURE 1: The MIMA tracker located in the installation tunnel inside the Palazzone Necropolis warehouse.

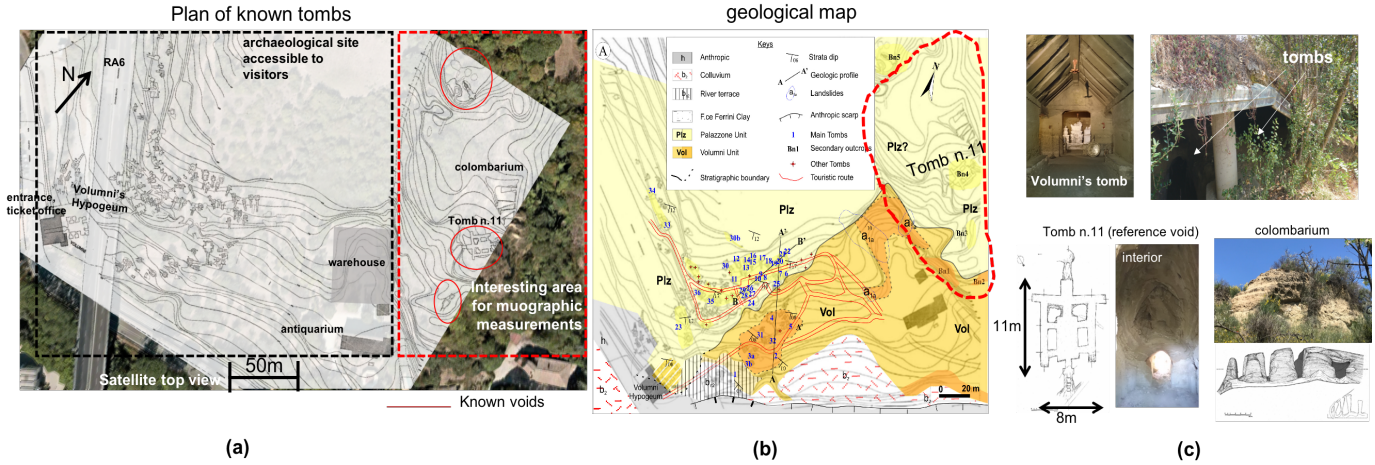

FIGURE 2: (a) The top view of the Palazzone Necropolis with the map of the known voids. The area open to the public is the West; the area that cannot be visited but is of interest for muographic measurements is to the East. (b) The geological map (taken from [21]) of the necropolis area in which the two main lithologies are highlighted: the Volumni unit and the Palazzone unit. (c) Some images of tombs: above, the Volumni Hypogeum and the entrance to some tombs accessible from the tourist route are visible; below, Tomb n. 11 and the *columbarium* in the area of muographic interest are shown. Tomb n. 11 represents the reference void for muographic measurements.

The necropolis of Palazzone can ideally be divided into two parts (Figure 2(a)): the western area, which is better known and open to the public, and the eastern area, which is partially known and not open to the public. The eastern area, although not yet included in the archaeological park, contains some archaeological structures: Tomb n. 11 which has an articulated shape similar to the Hypogeum of the Volumni, the columbarium, which is a partially collapsed structure, which allowed the deposition of some remains (Figure 2(c)), and in the area at south of Tomb n. 11, two other tombs are observed with collapsed ceilings. In the northern area, the presence of archaic tombs is known but they have not yet been geolocalized due to the dense vegetation. This area not accessible to visitors is precisely the area of interest from the point of view of the muographic surveys for the search for tombs whose existence is certain from the literature but has not yet been found. Furthermore, Tomb n. 11 represents the known void on which one can crosscheck the results of the technique in this archaeological application.

4. FEASIBILITY STUDY

Before the measurement at the archaeological site, a feasibility study was carried out to estimate a suitable installation point and to estimate the necessary acquisition time. The area of interest stands on a hill characterized by a height difference of about 45 m. In order to take advantage of the relation seen in Section 1, that is, $\Phi \propto \cos^2(\theta)$, it is important to find an installation point from which the area of interest is seen from an elevation angle ($\alpha = 90 - \theta$) as large as possible.

From a logistical point of view, the best place for installation due to the availability of power mains and ethernet network resulted in the warehouse structure. This structure is partly underground and the lower floor is about 10 m below the hill's surface. Preliminary simulations were therefore made by positioning the detector inside the warehouse and pointing it in the direction of the hill toward Tomb n. 11, at an elevation angle of 45°. To estimate the required measurement time, the void relating to Tomb n. 11 was taken as a reference, which was schematized, in this preliminary simulation, with a parallelepiped that reproduces it approximately in size and position. The geometry of the hill was acquired via Laser imaging Detection and Ranging (LiDAR) with a resolution of $(1 \times 1)\,\mathrm{m}^2$. Also, the distant geographical features are included by taking a Digital Terrain Model (DEM) with a resolution of $(5 \times 5)\,\mathrm{m}^2$. The details of the geometry used in the simulation are found in Figure 3(a). The simulation tool used is a custom tool [23] based on an atmospheric muon generator calibrated on the data acquired by the magnetic spectrometers ADAMO [25] and DEIS [26], and the interaction of muons with the matter is calculated by using the tabulated values present in the literature [27]. Two simulations of data collection lasting 14 days were carried out: the first one including the volume reproducing the tomb and the second one without this volume. The transmissions $t_{\text{with-tomb}}$, derived from the first simulation, and $t_{\text{without-tomb}}$, derived from the second one, have been used to obtain the relative transmission T_{relative} in order to highlight the presence of the tomb:

$$T_{\text{relative}} = \frac{t_{\text{with-tomb}}}{t_{\text{without-tomb}}}, \tag{2}$$

where t is the muon transmission defined in Section 1. In Figure 3(b), the relative transmission distribution obtained from the simulations described above is reported. After 14 days of data taking with the MIMA detector inclined at 45° of elevation, Tomb n. 11 should therefore be visible with a difference of transmission with respect to the surrounding areas of 25–30%. Furthermore, the tomb can be seen under elevation angles of about 20°, and therefore, in order to maximize acceptance in this direction, it was decided, during the measurement phase, to point the detector at this elevation value. Any other tombs may be located at similar or lower values of elevation angles; therefore, the data acquisition time will have to be greater than that used for the preliminary simulation. It was observed that even distant mountains can influence the measurement at elevation angles below about 10°.

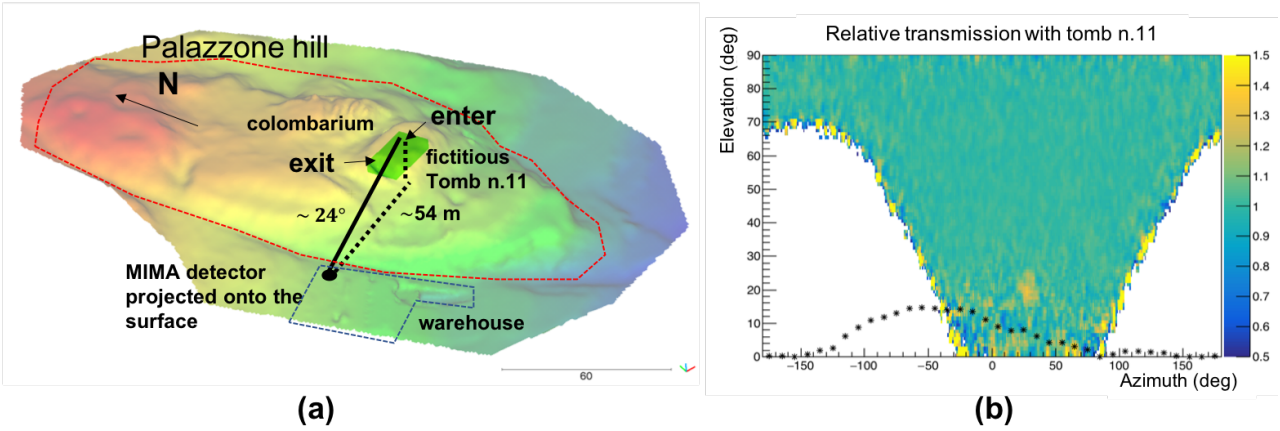

FIGURE 3: (a) The geometry used for a preliminary simulation in which a fictitious volume that reproduces Tomb n. 11 (the reference void) was inserted. The colors indicate the altimetry of the observation hill. (b) The relative transmission map obtained with a simulation of data collection lasting 14 days with the MIMA detector in the warehouse, pointed in the direction of Tomb n. 11 and oriented at 45°. The black-dotted plot denotes the profile of the distant hills as seen by the detector.

5. TWO-DIMENSIONAL IMAGING AT THE PALAZZONE NECROPOLIS: RESULTS

The two-dimensional angular results obtained with the muon imaging procedure described in Section 1 to search for voids within the area of interest of the Palazzone Necropolis are reported. At the Palazzone Necropolis, only one muographical measurement has currently been carried out which has made it possible to estimate, through a blind data analysis procedure, the areas with the greatest probability of finding any accesses to the searched cavities. A preliminary successive on-field inspection allowed us to highlight a good correspondence of the muographic results with the voids that develop from the surface. Furthermore, the results will be interpreted taking into account the geological context of the Palazzone site.

5.1. Measured Muon Transmission

A single muographic measurement was carried out at the Palazzone Necropolis with the detector pointed at an elevation angle of 20° and oriented perpendicular to the wall of the warehouse (Figure 1) which looks toward the area of interest (azimuth ~ 41.2°). Figure 4(a) shows the position of the detector in the warehouse projected on the surface. In Figure 4(b), the map of the detected tracks $N_\mu(\theta, \varphi)$ in the target configuration after a data collection of about two months is reported. During the data taking, the status of the detector (operation, environmental conditions, and efficiency of the detecting planes) was monitored thanks to a

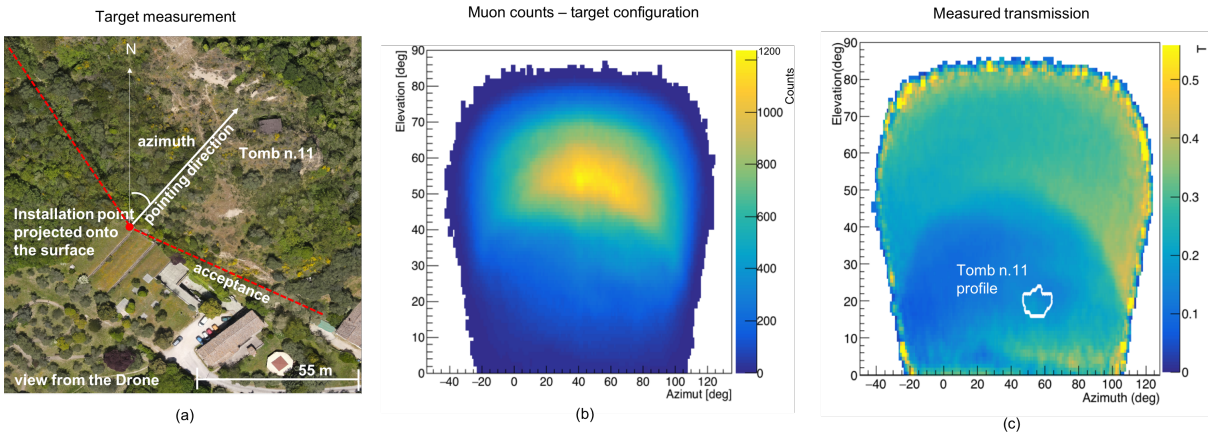

FIGURE 4: (a) The installation point projected onto the roof of the warehouse. In (b) and (c), respectively, the angular maps of detected tracks $N_\mu(\theta, \varphi)$ in the target configuration and the measured transmission $t_{\text{meas}}(\theta, \varphi)$ obtained from the comparison of the target and free-sky measurements. A linear smoothing filter was applied to the two distributions.

remote connection. A series of on-field campaigns performed with laser scanner, drone, and GPS mapping were carried out during the data taking in order to obtain the precise location and orientation of the detector inside the warehouse and to acquire as precise as possible the geometry of the area of interest. During these campaigns, a point cloud of Tomb n. 11 was also acquired, in order to verify the alignment between the measurement and the simulation. The reference measurement in the free-sky configuration was carried out in the following months on the roof of the INFN (National Institute of Nuclear Physics) building in Florence due to the impossibility of a view free from mountains or hills in the area around the necropolis. The free-sky flux was obtained by pointing the detector at an elevation angle of 20° in a South direction without distant hills.

The target and free-sky measurements, being performed in two different geographical locations (the first one in Perugia and the second one in Florence, with a distance of approximately 120 km) with different geographical features, differ in latitude and longitude ($\delta \sim [(-39°)_{\text{lat}}, (+1°28°)_{\text{long}}]$) and in the azimuth pointing direction $(138°)$. The former brings a negligible variation effect on the cosmic ray flux [7]; the latter, closely linked to the East-West effect, can lead left-right difference in the measured fluxes of about 20%. The free-sky measurement is affected by the East-West effect which mainly concerns the low-energy muons [7], and therefore, before making the comparison with the target measurement, a symmetrization procedure was carried out for the free-sky tracks. The symmetrization procedure took place with respect to the pointing direction by applying a reflection with respect to the azimuth angle.

From the comparison between the target measurement and the free-sky measurement (equation (1)) we obtain the measured transmission of Figure 4(c) which also shows the profile of Tomb n. 11. It can be observed that the target hill is visible at elevation angles below about 50°, and it can be observed how this decreases from North to South compatibly with the trend of the hill (visible in Figure 3(a)) which, rising in altitude to the North, presents more material in these directions. Furthermore, the profile of Tomb n. 11 overlaps with a high transmission area, indicating a good alignment between the measurement and the real position of the reference tomb.

5.2. *Simulations*

For the simulation, it is necessary to use a geometry as realistic as possible. In the case study of the Palazzone Necropolis, the surface is covered by a dense layer of vegetation (Figure 5(a)) which has a negligible effect on muon transmission. This layer must be eliminated in the target geometry used for simulations in order to have no artifacts in comparison with the measurement. Thanks to the geometries of the observation hill already available [28, 29] and to the laser scanner, drone, and GPS campaigns carried out at the Palazzone Necropolis, it was possible, through their comparison and their merging, to construct a precise geometry despite the thick vegetation that covers almost the entire hill of interest [24]. The GPS points were taken as a reference for the estimation of the geometry error acquired for the simulation which turned out to be approximately ± 50 cm in vertical direction. Figures 5(b) and 5(c), respectively, show the geometry of the simulation and the simulated transmission distribution for a homogeneous density of the hill of 2.1 g/cm^3 in the density range of the materials that make up the hill. The simulation carried out for the generation of this distribution is a *custom* simulation in which the effect of multiple scattering in the matter is not included.

Before proceeding to the generation of the angular distributions of average density, we evaluated how much the error of ± 50 cm on the geometry can affect the muographic images [24]. The difference in material thickness observed from the MIMA point of view between the nominal case and the case of geometry fully raised by $z = 50$ cm was evaluated. The angular regions correspond to the areas of the surface in which the observation directions of the detector are perpendicular to the normals of the simulated surface; the difference in thickness of material encountered between the simulation and the real trend of the hill reaches values of the order of tens of meters generating artifacts. Figure 5(d) shows the outline of areas at greatest risk of artifacts with values between 1 m and about 10 m due to the difficult removal process of vegetation from the simulation geometry. Since the anomalies searched for

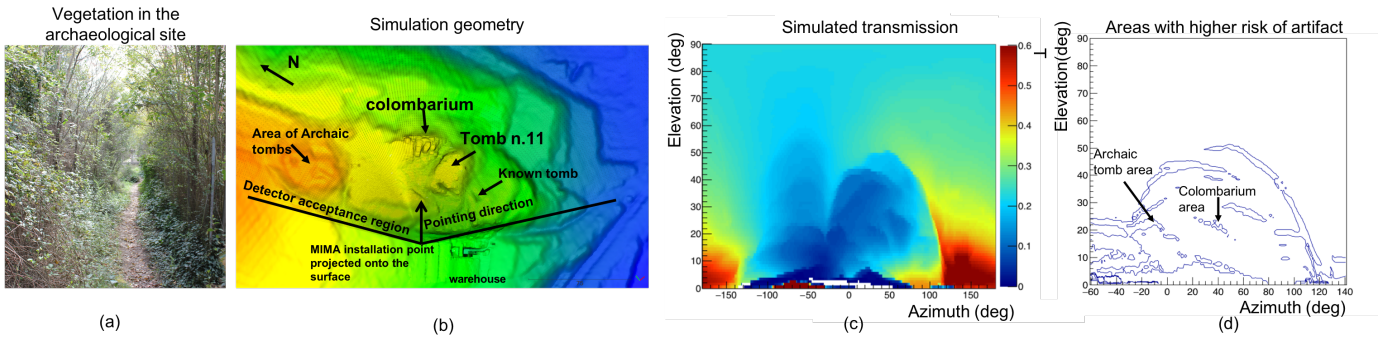

FIGURE 5: (a) A photograph of a stretch of road that runs along the Palazzone hill with thick vegetation. (b) The geometry used for the simulation after the removal of vegetation from the point clouds acquired with a laser scanner and drone campaigns. (c) The simulated transmission with a hill density of 2.1 g/cm^3. (d) The zones, in the detector acceptance, with the highest risk of artifacts due to the difficulty in removing the vegetation obtained by raising and lowering the geometry along z by ± 50 cm. This value was estimated based on a comparison between the geometry used for the simulation and the GPS points taken as reference.

(tombs) are of the same order of magnitude as the error due to the imperfect geometry of the hill, these areas will be excluded from the search for low-density anomalies.

5.3. *Density Distribution at the Palazzone Necropolis*

The two-dimensional angular density distribution was obtained, as described in Section 1, by comparing the measured transmission with the simulated one. The obtained average density distribution is reported in Figure 6(a). The overlap with the areas at greatest risk of artifacts in Figure 5(d) is also reported, and it can be observed that some low-density areas overlap with these. The *columbarium* area also has artifacts in the superficial part, due to the fact that, in the *columbarium* gorges, the vegetation has not been completely removed from the reconstructed geometry. This was also confirmed by a comparison with acquired GPS points. The arc-shaped low-density structure (denoted by **Arc** in Figure 6(a)) at high elevation angles is due to the presence of a corridor on the roof of the warehouse which is not present in the geometry of the simulation, and therefore, it is visible as if it were a cavity.

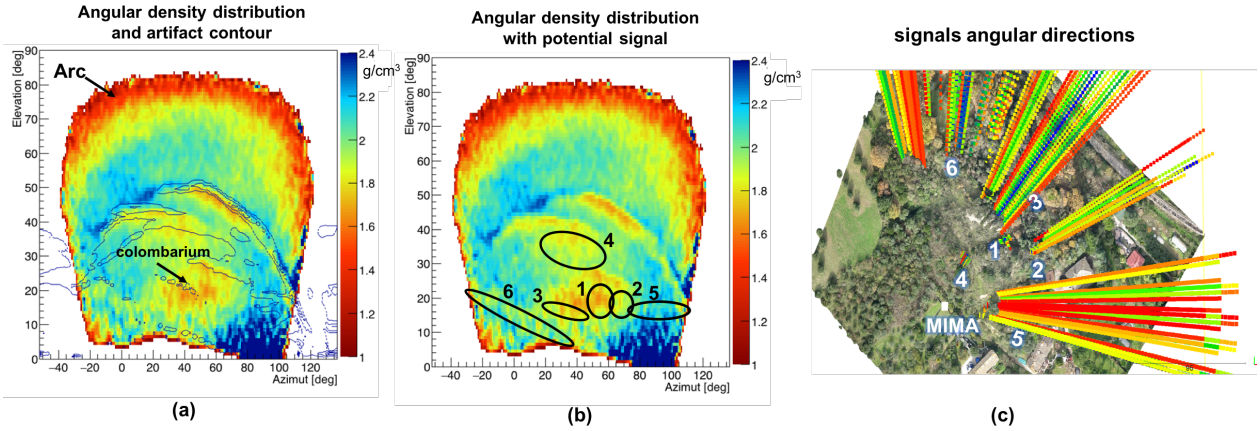

FIGURE 6: (a, b) The angular distribution of average density in which the angular areas at greatest risk of artifacts and the possible signals attributable to real cavities have been, respectively, highlighted. Low-density signal n. 1 is Tomb n. 11. In (c), the low-density angular directions as seen from the point of view of the detector are reported on the Earth's surface.

The sensitivity on the density values found in the areas where there are no artifacts or cavities is about $\pm 0.1\,\mathrm{g/cm^3}$ estimated starting from a direct comparison with extracted material samples in the area and adding in quadrature the statistical error and the error due to the imperfect geometry of the simulation. This latter contribution equal to $\pm 0.03\,\mathrm{g/cm^3}$ was estimated considering a geometry with a vertical error of $z = \pm 50$ cm (in the same way as the estimation of the areas defined as artifacts described previously). In areas where the detector's observation directions are parallel to the surface (artifacts) and therefore the error associated with the topology is larger, errors in the density values found can reach up to $\pm 0.6\,\mathrm{g/cm^3}$.

The obtained average density values, excluding the artifacts, are compatible with the range of values expected from lithological knowledge. It can also be observed that in the East direction, under elevation angles of 15°, the density values are slightly higher than in the rest of the map. This may be due to the presence of the Volumni unit (slightly denser than the Palazzone unit) in this area and to the presence of some buildings below ∼5°.

5.4. A Preliminary Estimation of the Areas with a Higher Probability of Containing Cavities

Being interested in the search for cavities and excluding the areas with artifacts, it is possible to identify in Figure 6(b) some low-density angular regions indicated by a number between 1 and 6 which may point out the presence of cavities. These signals were identified by looking for the lowest density areas respect with the neighboring angular regions by inserting cuts on the density. Region n. 1 corresponds to the reference Tomb n. 11. This distribution only gives us two-dimensional information, and we do not know how far away from the detector they are. To obtain three-dimensional information, other measurements are generally carried out on the same site and the triangulation technique can be applied.

Preliminary, it is possible to identify the areas most likely to have cavities by combining the information obtained from the two-dimensional distribution of average density with the knowledge of the Etruscan method of excavating tombs in the Hellenistic and Archaic periods. In particular, the Etruscans in the Hellenistic age, in analogy to the tombs present in the archaeological site open to the public, excavated a horizontal corridor called *dromos* from the surface which led to the completely buried body of the tomb. The *dromos* can be a few meters long and can have a slight downward slope. Surface areas with a higher probability of cavity access can be identified by drawing rays that start from the center of the detector in the target measurement and travel in the directions of view identified by the low-density bins (Figure 6(c)). The areas of the surface where the rays intersect are then sought. Some of these rays head toward Tomb n. 11, toward the north where archaic tombs are being sought, and the southern area where there are two known tombs with collapsed ceilings. Other signals not attributable to known voids were also identified. In cases where the point of installation and the conformation of the site are such that the rays, traveling in depth, intersect the surface only once, this procedure allows for limiting the areas where it is most likely to find access. Otherwise, for example, if the ray crosses the surface two or three times, the potential signal areas can double or triple. In the particular case of the Palazzone Necropolis, all the rays intersect the surface only once. This procedure can be further optimized by knowing the thickness of air associated with each low-density signal. Knowing the thickness of air and knowing that the tombs sought are all underground, it is possible to exclude some areas from others and also to estimate the depth to which they reach.

Figure 7(left) shows the areas identified in the archaeological site of Palazzone as the areas most likely to find access to cavities. After a very preliminary inspection, good correspondences were found with holes partially covered by vegetation and soil that could correspond to entrances to tombs. In Figure 7(right), some images are shown. Further inspections are planned in these areas with the collaboration of archaeologists. It was not possible to access some areas due to the very dense vegetation. More targeted inspections will be carried out in the future by a team of archaeologists.

FIGURE 7: *Left*: the areas most likely to find access to cavities are shown, obtained by combining muographic results with knowledge of the Etruscan excavation technique. *Right*: a series of photographs depicting some surface voids found in these areas during a preliminary inspection are reported.

6. DISCUSSIONS

Given the complex geometry of the observation site due to the dense vegetation present and the unfavorable measurement conditions: low elevation angles, large detector-target distances (up to 120 m), and relatively small anomalies (below 10 m), before searching for anomalies linked to the presence of tombs, it was necessary to evaluate the contribution of the reconstructed imperfect geometry of the observation area to the muographic images.

Various point cloud acquisition campaigns were carried out with different close-range remote sensing methods to create the geometry that better reproduced the observation hill after the removal of the vegetation. The details of this procedure can be found in [24]. Through the acquisition of GPS points with centimeter precision taken as reference, it was possible to evaluate the average deviation between the geometry chosen for the simulation and the real development of the hill.

It has been observed that an average vertical deviation of 50 cm can lead, for certain detector directions of view, to differences in material observed along the line of sight of up to 10 m. These values are of the same order of magnitude as the extension of the cavities sought and therefore the errors are not negligible for this type of application. The viewing directions most affected by this phenomenon are those parallel to the surface, and it is precisely in these angular regions that anomalous density values are observed with errors of up to $\pm 0.6\,\mathrm{g/cm^3}$. These angular areas referred to as artifacts were excluded from the analysis of possible cavity signals. Excluding artifacts, the density values have an error of about $\pm 0.1\,\mathrm{g/cm^3}$ and are compatible with those expected from previous geological studies of the area.

The intersections of the low-density angular regions with the Earth's surface were preliminary identified extending their angular directions in space and, given the superficial nature of the tombs researched, they identify the areas with the highest probability of finding cavities.

7. CONCLUSIONS AND FUTURE DEVELOPMENTS

This article reports a preliminary muographic study within the archaeological site of the Palazzone Necropolis located in Perugia (Italy). The measurement was concentrated on a still partially known area of the necropolis and involved the search, through muographic imaging, for the presence of undiscovered voids. The measurement was carried out by pointing the detector at low elevation angles (20°). The acquisition time was about two months. The application of the noninvasive technique of muography in this archaeological site was affected by some problems related to the presence of dense vegetation which led to the identification of artifacts in the maps generated despite the careful search procedure for the best geometry that would reproduce, for the simulations, the observation hill. The two-dimensional angular distribution of average density obtained has values that are compatible with the materials that make up the target hill. Some low-density areas have been highlighted as areas with the potential presence of cavities. In particular, the known void of Tomb n. 11, taken as a reference, was identified in the correct direction. Preliminarily, the areas on the Earth's surface most likely to contain accesses to voids were estimated by combining the two-dimensional angular average density distribution by extending the low-density directions observed by the detector and taking into account the technique used in the Etruscan age to build tombs.

Currently, in order to have a more precise three-dimensional localization, the reconstruction with the back-projection technique [12] of the low-density signals and the estimation of the thickness of air of these signals is in progress. Further on-site inspections are planned in the future for the direct localization of these unknown voids identified with the muon transmission muography technique.

CONFLICTS OF INTEREST

The authors declare that there are no conflicts of interest regarding the publication of this paper.

References

[1] L. W. Alvarez et al., *Search for Hidden Chambers in the Pyramids*, Science **167** (1970) 832. DOI: 10.1126/science.167.3919.832.

[2] F. Ambrosino et al., *The MU-RAY project: detector technology and first data from Mt. Vesuvius*, JINST **9** (2014) C02029. DOI: 10.1088/1748-0221/9/02/C02029.

[3] M. D'Errico et al., *The MURAVES muon telescope: a low power consumption muon tracker for muon radiography applications*, J. Phys., Conf. Ser. 2374 (2022) 012190. DOI:10.1088/1742-6596/2374/1/012190.

[4] V. Tioukov, A. Alexandrov, C. Bozza et al., *First muography of Stromboli volcano*, Sci Rep **9** (2019) 6695. DOI: 10.1038/s41598-019-43131-8.

[5] L. Oláh, G. Gallo, G. Hamar et al., *Muon Imaging of Volcanic Conduit Explains Link Between Eruption Frequency and Ground Deformation*, Geophysical Research Letters **50** (2023) e2022GL101170. DOI:10.1029/2022GL101170.

[6] P. A. Zyla et al. (Particle Data Group), *Review of Particle Physics*, PTEP 2020 (2020) 083C01. DOI: 10.1093/ptep/ptaa104.

[7] P. K. Grieder, *Cosmic rays at Earth*, Elsevier (2001).

[8] A. Tarantola, *Inverse Problem Theory and Methods for Model Parameter Estimation*, SIAM (2005). DOI: 10.1137/1.9780898717921.

[9] M. Rosas-Carbajal et al., *Three-dimensional density structure of La Soufrière de Guadeloupe lava dome from simultaneous muon radiographies and gravity data*, Geophys. Res. Lett., **44** (2017) 6743. DOI:10.1002/2017GL074285.

[10] G. Baccani, *Muon absorption tomography of a lead structure through the use of iterative algorithms*, JINST **15** (2020) P12024 DOI: 10.1088/1748-0221/15/12/P12024.

[11] G. Baccani, *Development, testing and application to a real case studies of a three-dimensional tomographic technique based on muon transmission radiography*, P.h.D. Thesis in Physics and Astronomy, University of Florence (2020).

[12] L. Bonechi et al., *A projective reconstruction method of underground or hidden structures using atmospheric muon absorption data*, JINST **10** (2015) P02003. DOI: 10.1088/1748-0221/10/02/P02003.

[13] D. Borselli, T. Beni, L. Bonechi et al., *Three-dimensional muon imaging of cavities inside the Temperino mine (Italy)*, Sci. Rep. **12** (2022) 22329. DOI: 10.1038/s41598-022-26393-7.

[14] T. Beni, D. Borselli, L. Bonechi et al., *Transmission-Based Muography for Ore Bodies Prospecting: A Case Study from a Skarn Complex in Italy*, Nat. Resour. Res. **32** (2023) 1529. DOI: 10.1007/s11053-023-10201-8.

[15] G. Baccani et al., *The MIMA project. Design, construction and performances of a compact hodoscope for muon radiography applications in the context of Archaeology and geophysical prospections*, JINST **13** (2018) no. 11, P11001. DOI: 10.1088/1748-0221/13/11/P11001.

[16] G. Baccani, *Construction and calibration of the MIMA cosmic ray tracker for applications related to muon radiography and first measurements*, Master's Thesis in Physical and Astrophysical Sciences, Fac. Math. Phys. Nat. Sci., University of Florence (AA 2016/2017).

[17] G. Baccani et al., *Muon Radiography of Ancient Mines: The San Silvestro Archaeo-Mining Park (Campiglia Marittima, Tuscany)*, Universe **5** (2019) 34. DOI: 10.3390/universe5010034.
[18] L. Cimmino et al., *3D Muography for the Search of Hidden Cavities*, Sci Rep **9** (2019) 2974. DOI: 10.1038/s41598-019-39682-5.
[19] G. Baccani et al., *The reliability of muography applied in the detection of the animal burrows within River Levees validated by means of geophysical techniques*, Journal of Applied Geophysics **191** (2021), 104376. DOI: 10.1016/j.jappgeo.2021.104376.
[20] R. De Rubertis, *Rilievi archeologici in Umbria. Perugia, Assisi, Orvieto, Otricoli, Spoleto*, ESA (Torre del Greco) (2012).
[21] R. Bizzarri, L. Melelli, and C. Cencetti, *Archaeo-geosites in urban areas: a case study of the etruscan Palazzone necropolis (Perugia, central Italy)*, Alpine and Mediterranean Quaternary **31** (2018) 207–219. DOI: 10.26382/AMQ.2018.15.
[22] L. Melelli, R. Bizzarri, A. Baldanza, and L. Gregori, *The Etruscan "Volumni Hypogeum" Archeo-Geosite: New Sedimentological and Geomorphological Insights on the Tombal Complex*, Geoheritage, **8** (2016) 301–314. DOI: 10.1007/s12371-015-0162-z.
[23] S. Gonzi et al., *A parametric analytical model of the atmospheric muon flux at sea-level and its application in the field of the muon transmission radiography*, PoS ICRC2023 (2023) **526**. DOI: 10.22323/1.444.0526.
[24] T. Beni et al., *Laser scanner and UAV digital photogrammetry as support tools for cosmic-ray muon radiography applications: an archaeological case study from Italy*, Sci Rep **13**, 19983 (2023). DOI:10.1038/s41598-023-46661-4
[25] L. Bonechi, *Measurements of Cosmic Rays at Earth with the Experiment ADAMO*, Ph.D. Thesis in Physics and Astronomy, University of Florence (2004).
[26] O. C. Allkofer et al., *Cosmic-ray muon spectra at sea-level up to 10 TeV*, Nucl. Phys. B **259** (1985), 1 DOI: 10.1016/0550-3213(85)90294-9 [erratum: Nucl. Phys. B 268 (1986), 747. DOI: 10.1016/0550-3213(86)90270-1].
[27] D. E. Groom et al., *Muon stopping power and range tables 10-MeV to 100-TeV*, Atom. Data Nucl. Data Tabl. **78** (2001), 183–356. DOI: 10.1006/adnd.2001.0861.
[28] University of Perugia and Fondazione Cassa di Risparmio di Perugia, SILENE Project (website). http://silenepg.it / Accessed September 09, 2023.
[29] DTM lidar 1 meter ground resolution, Ministero dell'Ambiente e della tutela del Territorio e del Mare-Rilievi Lidar. Umbria Region (website) http://www.pcn.minambiente.it/viewer/index.php?, Accessed September 09, 2023.